Supplementary Information

The log-logistic evolution of meteorite friability and implications for asteroid regolith

Suraj Bhatt[1], Laurence A. J. Garvie[2,3], Desireé Cotto-Figueroa[4], Erik Asphaug[5], Christian G. Hoover [1*]

[1]School of Sustainable Engineering and the Built Environment, Ira A. Fulton Schools of Engineering, Arizona State University, Tempe, AZ 85287, United States. [2]Buseck Center for Meteorite Studies, Arizona State University, Tempe, AZ 85287-6004, United States. [3]School of Earth and Space Exploration, Arizona State University, Tempe, AZ 85287-6004, United States. [4]Department of Physics and Electronics, University of Puerto Rico at Humacao, Call Box 860, Humacao, PR 00792, Puerto Rico, United States. [5]Lunar and Planetary Laboratory, University of Arizona, Tucson, AZ 85721, United States.

* Corresponding author (Christian.Hoover@asu.edu)

Supplementary Discussion

The fragmentation behavior of Richardton, the most friable of the meteorites studied, is tied to its distinct lithological characteristics. The material retained on sieves #20, #40, and #60 corresponds to the size range of the chondrules (Supplementary Notes, Supplementary Table 2), suggesting that it fragmented preferentially along matrix-chondrule boundaries into chondrule-sized pieces. Tamdakht exhibits strong mechanical integrity across all sets of tumbling revolutions. Its chondrule size distribution (Supplementary Table 2) shows mass retention peaks at sieves #20, #40, and #60, indicative of chondrule-sized fragments, although to a lesser extent than in Richardton. The chondrules in Tamdakht are largely integrated into the matrix due to the thermal metamorphism[1], which welded the matrix and inclusions into a cohesive whole. As a result, during tumbling, the sample resists fragmentation because cracks cannot easily propagate along the indistinct chondrule-matrix boundaries. Visual inspection of the post-tumbling residues (Supplementary Fig. 3, 4) reinforces the distinction: Richardton disaggregated into sand and dust-sized matter, while Tamdakht preserved its pebble size with minimal surface abrasion.

Zhob and New Concord exhibit medium fragmentation behavior, despite having structurally distinct lithologies. Zhob shows prominent mass retention in sieves #20, #40, and #60 (Supplementary Table 2, Supplementary Fig. 5). This fragmentation behavior reflects its chondrule size range, indicating that fragmentation initially occurs around the chondrule boundaries. The dust accumulation in Zhob reflects the progressive disaggregation of its fine-grained, poorly cohesive matrix. This behavior indicates that fragmentation is not confined to chondrule-scale failure but extends to the release of matrix material, marking a transition from intergranular to intramatrix mechanical breakdown. New Concord exhibits significant mass retention in sieves #20, #40, and #60 (Supplementary Table 2, Supplementary Fig. 6), consistent with chondrule-sized fragments, and accumulates substantial dust. This pattern indicates that mechanical failure occurs at the matrix–chondrule interface and within chondrules under prolonged stress. Both meteorites display limited fragmentation during early tumbling but generate substantial dust by 10^5 revolutions, suggesting that their matrices, though stronger than Richardton's, gradually succumb to cumulative mechanical degradation.

In Allende, fragmentation produced a pronounced shift toward finer particle sizes, indicating extensive comminution into dust. The particle-size shift and sieve pattern indicate that its friability is governed by the pervasive fine-grained matrix and by low cohesion at mineral–mineral contacts within chondrules and CAIs. The matrix disaggregates readily into dust, and weak intergranular bonds within inclusions progressively liberating sub-grain fragments under sustained tumbling. CAIs and chondrules are abundant and large in Allende (mean 716 ± 460 µm; Supplementary Note), but the controlling factor is matrix fineness and weak intergranular cohesion, rather than splitting of the inclusions. This fragmentation behavior is further supported by the mass retention observed in sieves #20, #40, and #60 at lower revolution counts (Supplementary Table 2, Supplementary Fig. 9), corresponding to Allende's chondrule size range. However, as tumbling progresses, the retention in these sieves declines, indicating that the inclusions are gradually comminuted into the dust range.

Supplementary Notes

All mass retention patterns for all meteorites are shown in Supplementary Figs. 1-9 and Supplementary Table 2. Brief description of meteorite chondrule sizes are provided below:

Richardton (H5): Contains chondrules ranging from 0.2 to 2 mm[2], embedded in loosely bound olivine and monoclinic pyroxene crystals[3]. The coarse sieve bins (#20, #40, #60) correlate with this chondrule size range, suggesting that fragmentation occurred preferentially along chondrule–matrix boundaries. Richardton comprises ~80% silicates (mainly olivine and pyroxene) and ~20% Fe-Ni metal, and troilite, which form veins and contribute to mechanical heterogeneity.

Tamdakht (H5): Chondrules range from 0.1 to 1.5 mm and are well integrated into their recrystallized matrix. Thermal metamorphism in Tamdakht[1] welded the inclusions and matrix, inhibiting crack propagation. Its mineralogy includes olivine, orthopyroxene, chromite, minor clinopyroxene, Fe-Ni metal, and ilmenite[4].

Zhob (H3/4): Consists of well-defined chondrules averaging ~460 µm, set in a weakly consolidated fine-grained matrix. Lacks visible shock veins and is noted for ease of breakage[5]. Retention in sieves #20, #40, and #60 is consistent with chondrule-sized debris, but accumulation of <37 µm dust indicates progressive disaggregation beyond grain boundaries.

New Concord (L6): A high-petrologic grade chondrite with chondrules largely integrated into the matrix. Mineralogy is dominated by olivine, pyroxene, plagioclase, troilite, Fe-Ni metal, and chromite[6,7]. Exhibits both chondrule-sized and sub-37 µm fragmentation products.

Murchison (CM2): Features a fine-grained, phyllosilicate-rich matrix dominated by serpentine and saponite, with chondrules averaging 184 ± 173 µm and inclusions constituting ~28%[8,9]. Transmission electron microscopy (TEM) and STEM-FIB studies show an intergrown matrix of chrysotile, cronstedtite, and tochilinite, containing 2–5 nm Fe-Ni sulfide nanoparticles embedded within serpentine layers[10]. This nanostructure distributes deformation and suppresses crack propagation, imparting ductile toughness that resists mechanical disaggregation.

Aguas Zarcas (CM2): Shares a similar lithology with Murchison, including serpentine-dominated phyllosilicates intergrown with ferrotochilinite and embedded chondrules averaging ~275 µm[11,12]. The matrix architecture and mineralogical continuity with Murchison help explain its comparable resistance to friability. The limited mass redistribution into sand bins further supports this mechanical cohesion.

Allende (CV3): Inclusions constitute ~43% of the volume with chondrules averaging 716 ± 460 µm[8]. TEM and nano-CT analyses reveal CAIs are texturally complex, with porous interiors and zoned mineralogy[13]. The matrix is relatively coarse-grained (~5 µm), weakening cohesion[14–17]. Mass retention patterns indicate progressive breakdown of both inclusions and matrix.

Supplementary Figures

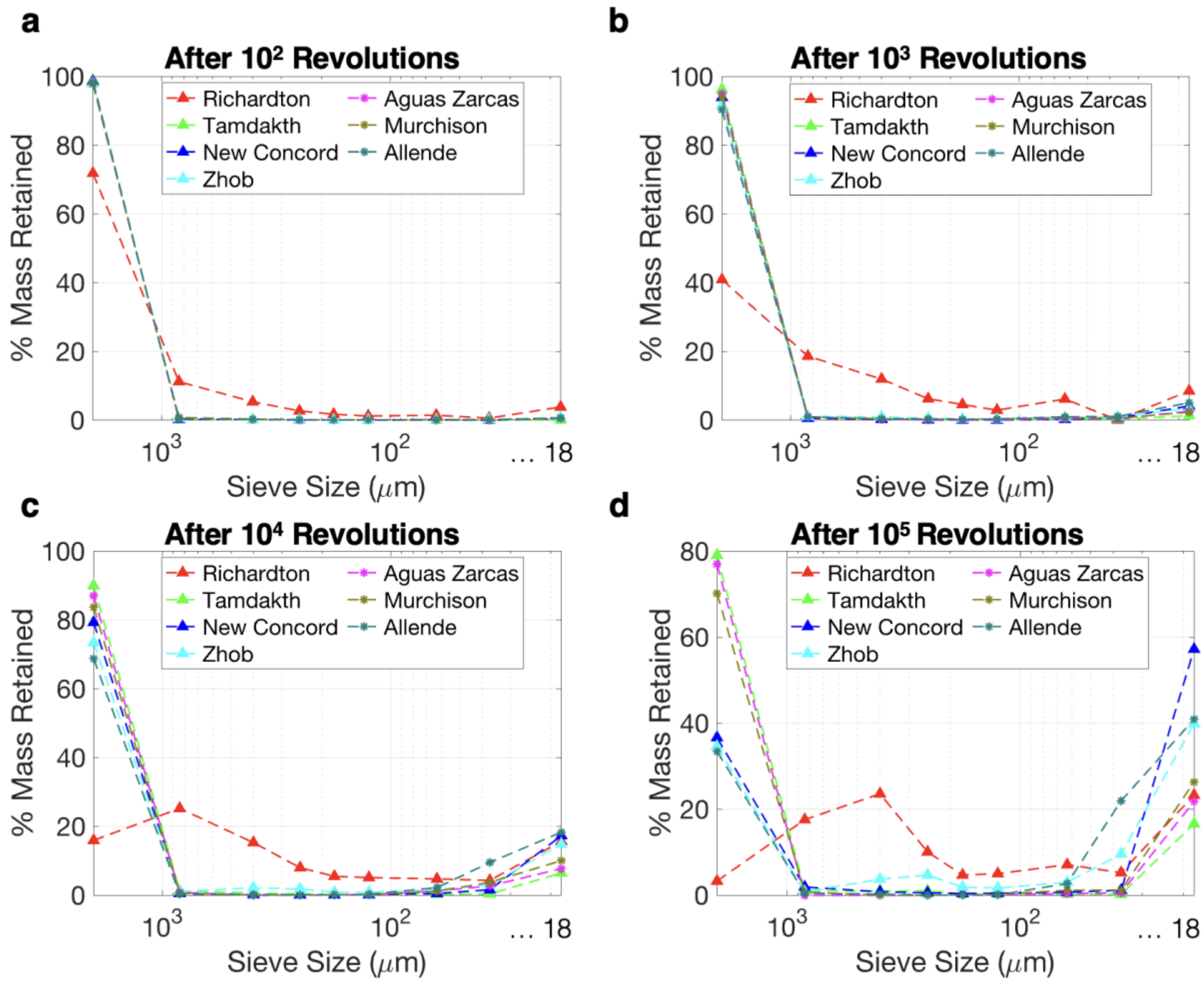

Supplementary Fig. 1: Evolution and final distribution of fragment sizes across the meteorites under progressive tumbling. a–d, Percent mass retained on each sieve size (largest sieve size is at the origin, x-axis is decreasing to the right in a logarithmic scale) after 10^2, 10^3, 10^4, and 10^5 revolutions, respectively, for all meteorite samples. Dust fractions (<37 μm) are plotted at 18 μm. Early fragmentation stages exhibit a loss of coarse edges, followed by a progressive increase in sand (37 μm–2 mm), a size range that encompasses typical chondrule diameters, large mineral fragments, and metal grains. The limited retention within this band reflects the incompatibility between primary chondritic textures and attrition-driven breakdown pathways. Triangles indicate ordinary chondrites, and stars indicate carbonaceous chondrites.

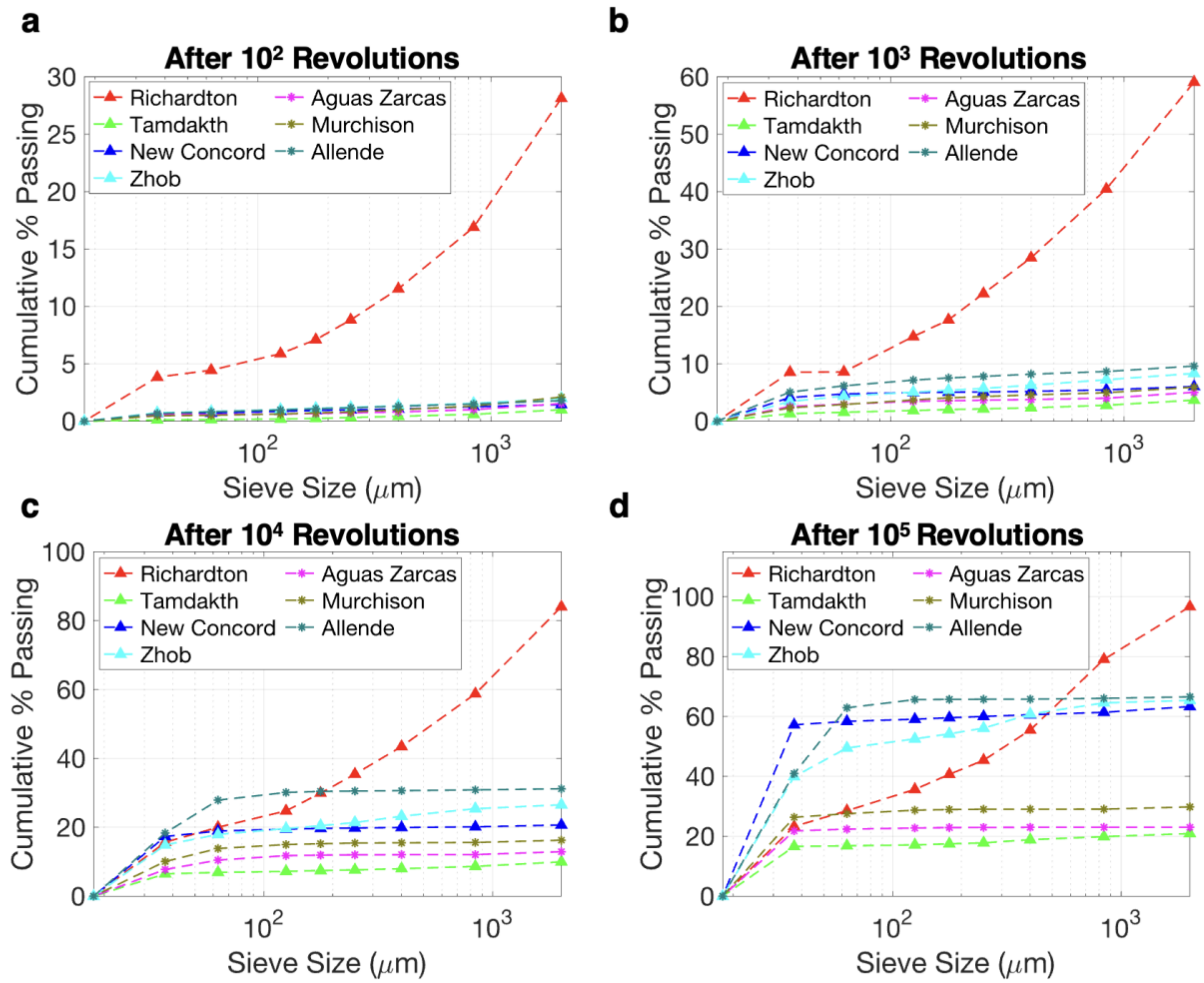

Supplementary Fig. 2: Fuller curves of meteorite fragments during progressive tumbling. Cumulative percent mass passing (Fuller curves) is plotted as a function of sieve opening size (μm) for each meteorite after **a**, 10^2, **b**, 10^3, **c**, 10^4, **d**, and 10^5 revolutions. Triangles indicate ordinary chondrites, and stars indicate carbonaceous chondrites.

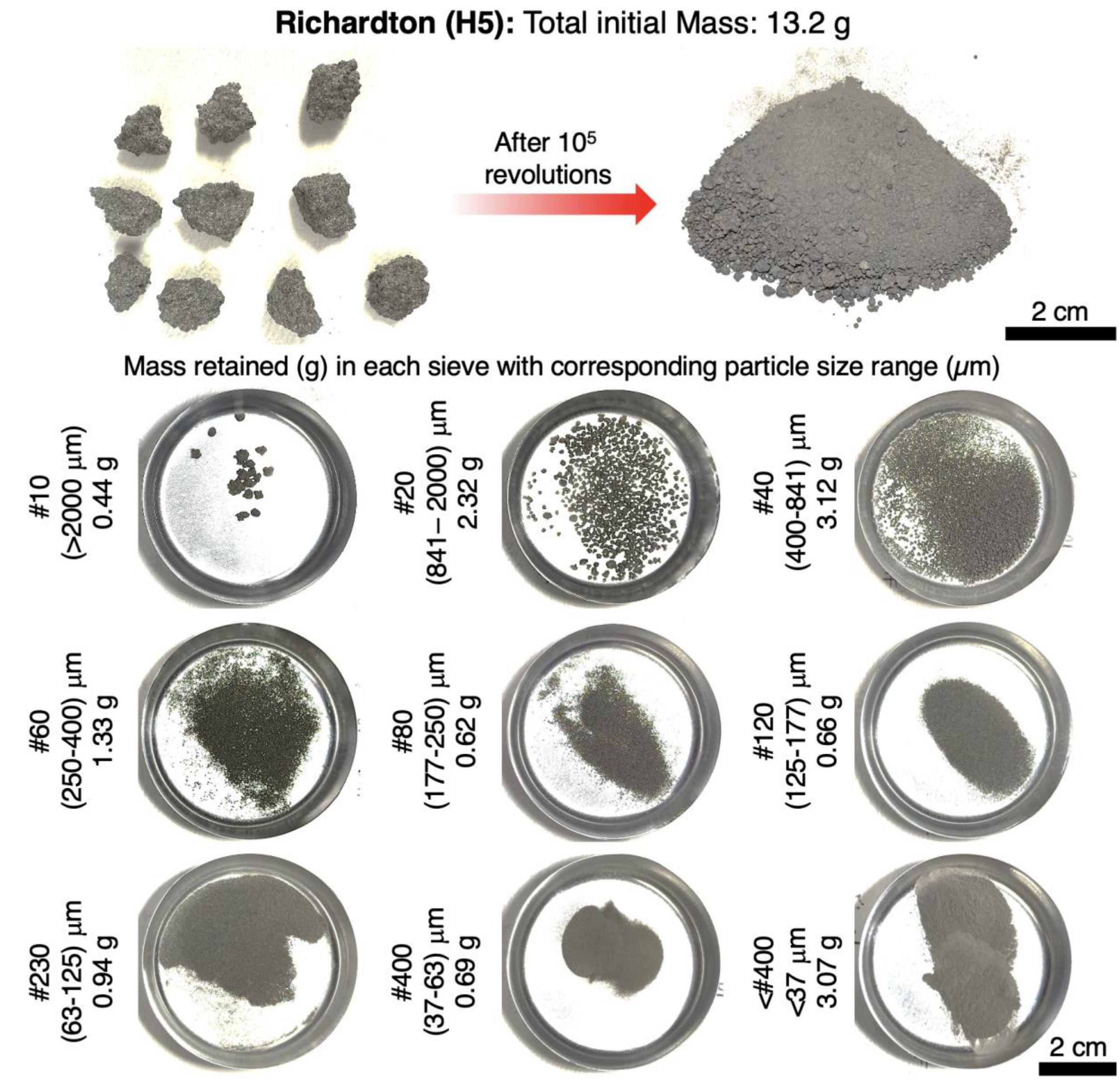

Supplementary Fig. 3: Particle-size distribution of the Richardton (H5, high friability) meteorite after 10^5 revolutions. Initial fragments (13.2 g) were subjected to mechanical tumbling until near-complete disaggregation. Post-experiment residue was separated by standard sieve analysis, and the mass retained in each sieve bin is shown alongside the corresponding particle size range. A substantial portion of the mass was redistributed into intermediate sand bins (63–841 μm), corresponding to typical chondrule sizes, with ~3.1 g classified as dust.

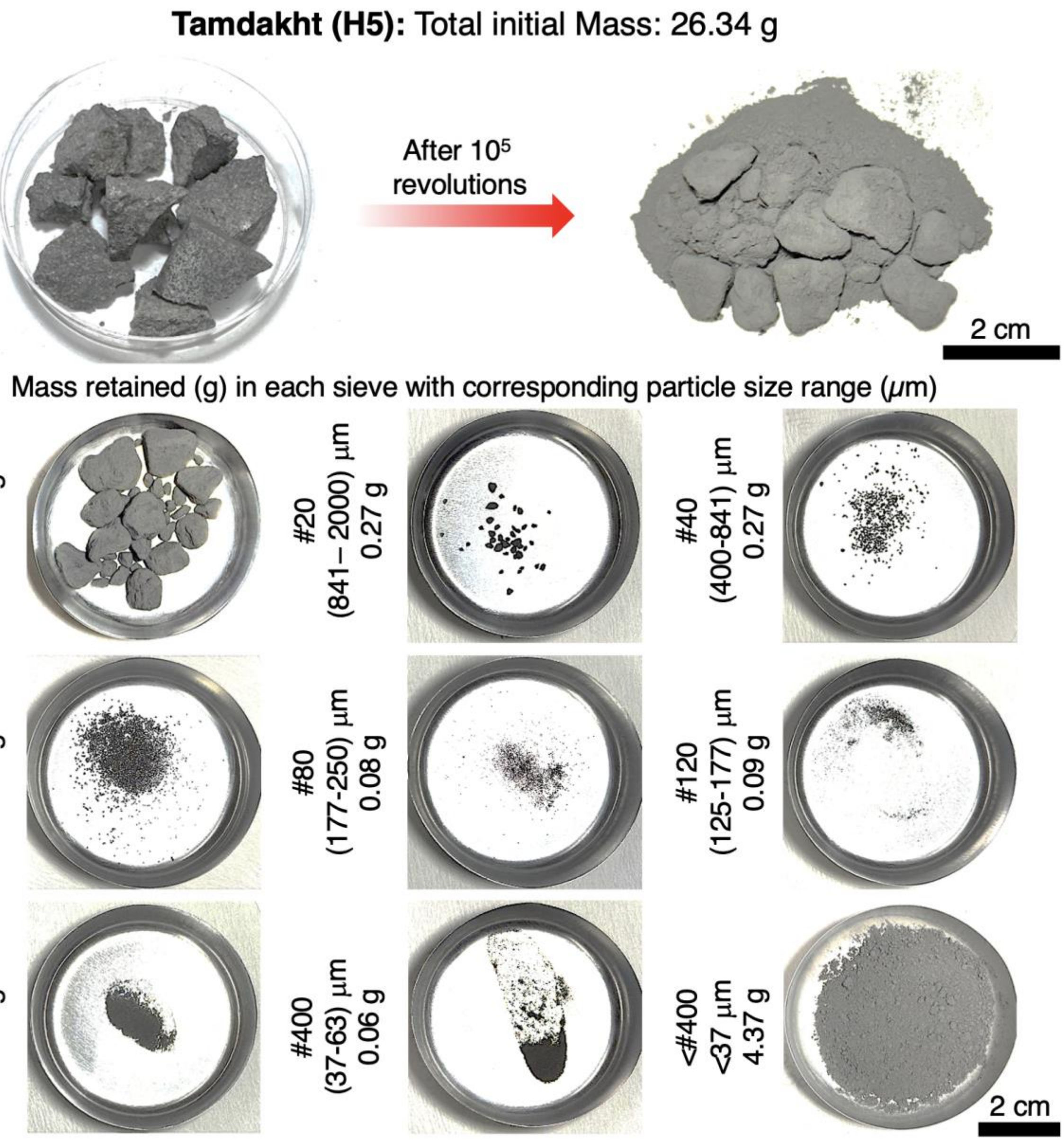

Supplementary Fig. 4: Particle-size distribution of the Tamdakht (H5, low friability) meteorite after 10^5 revolutions. A 26.34 g sample was subjected to mechanical tumbling and subsequently analyzed by sieve separation. The mass retained in each particle size bin is shown with the corresponding size ranges. Most material (~79%) remains in the pebble, indicating limited disaggregation.

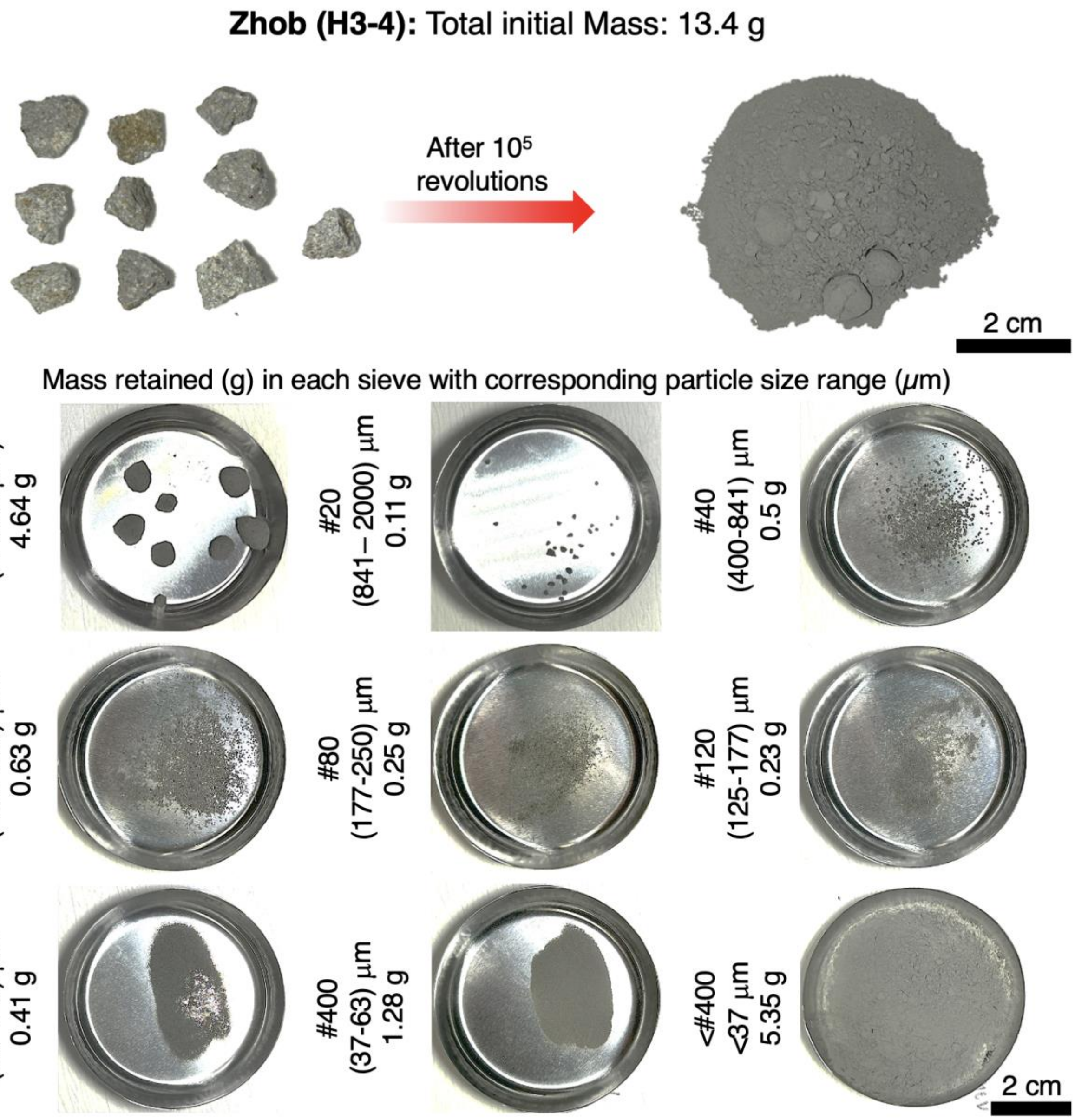

Supplementary Fig. 5: Particle-size distribution of the Zhob (H3-4, medium friability) meteorite after 10^5 revolutions. A 13.4 g sample was mechanically tumbled and analyzed by sieve separation. The mass retained in each bin is shown with the corresponding particle size ranges. Over 5.3 g of material passed below the 37 µm sieve, and ~1.3 g accumulated in the 37–63 µm bin, indicating widespread redistribution into sand and dust while retaining ~4.6 g in pebble.

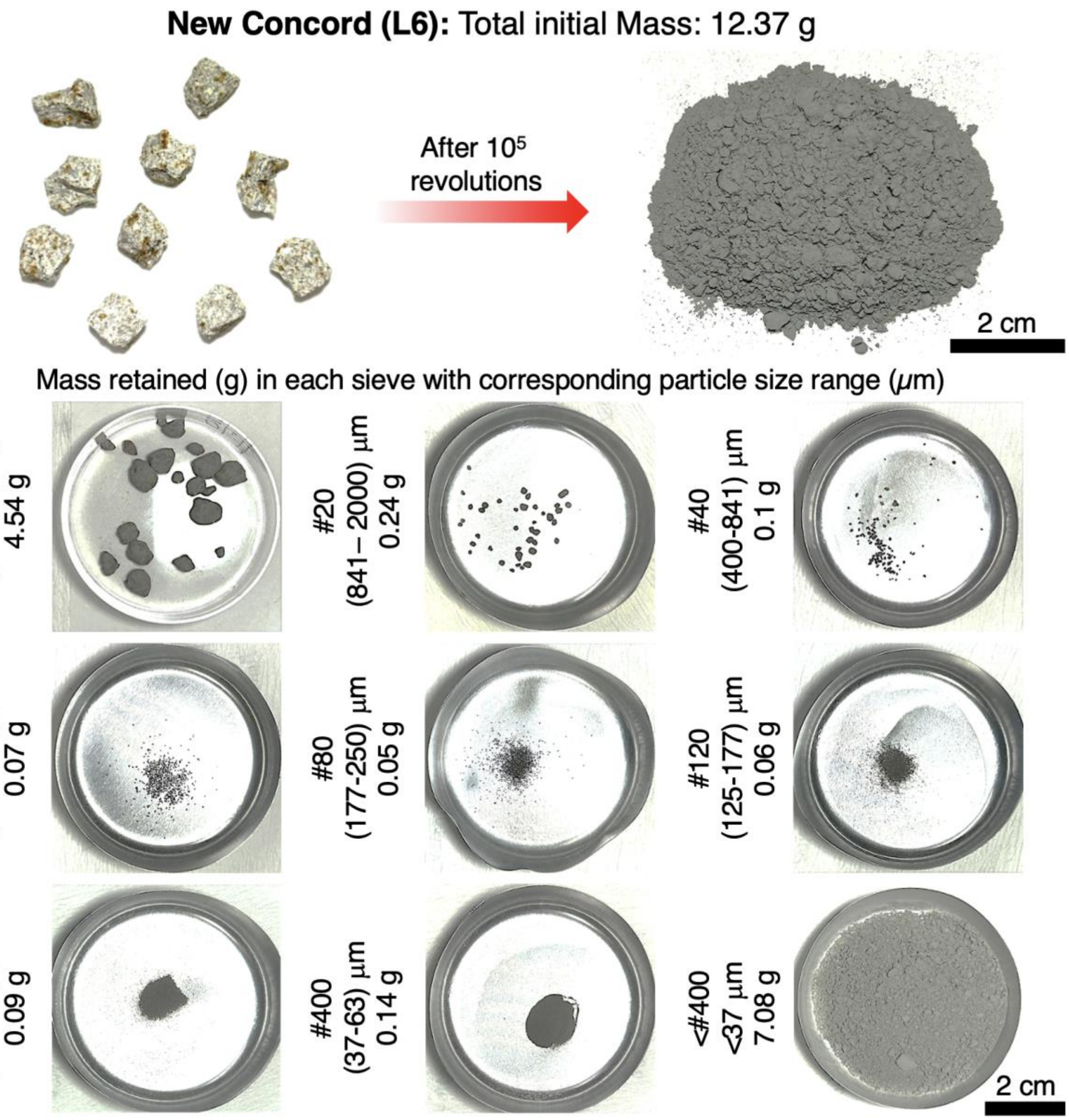

Supplementary Fig. 6: Particle-size distribution of the New Concord (L6, medium friability) meteorite after 10^5 revolutions. A 12.37 g sample was mechanically tumbled and separated by sieve analysis. The mass retained in each size fraction is shown with the corresponding particle size ranges. Despite partial retention of pebble (>2,000 μm), over 7 g of material was classified as <37 μm dust, indicating substantial disaggregation of the material.

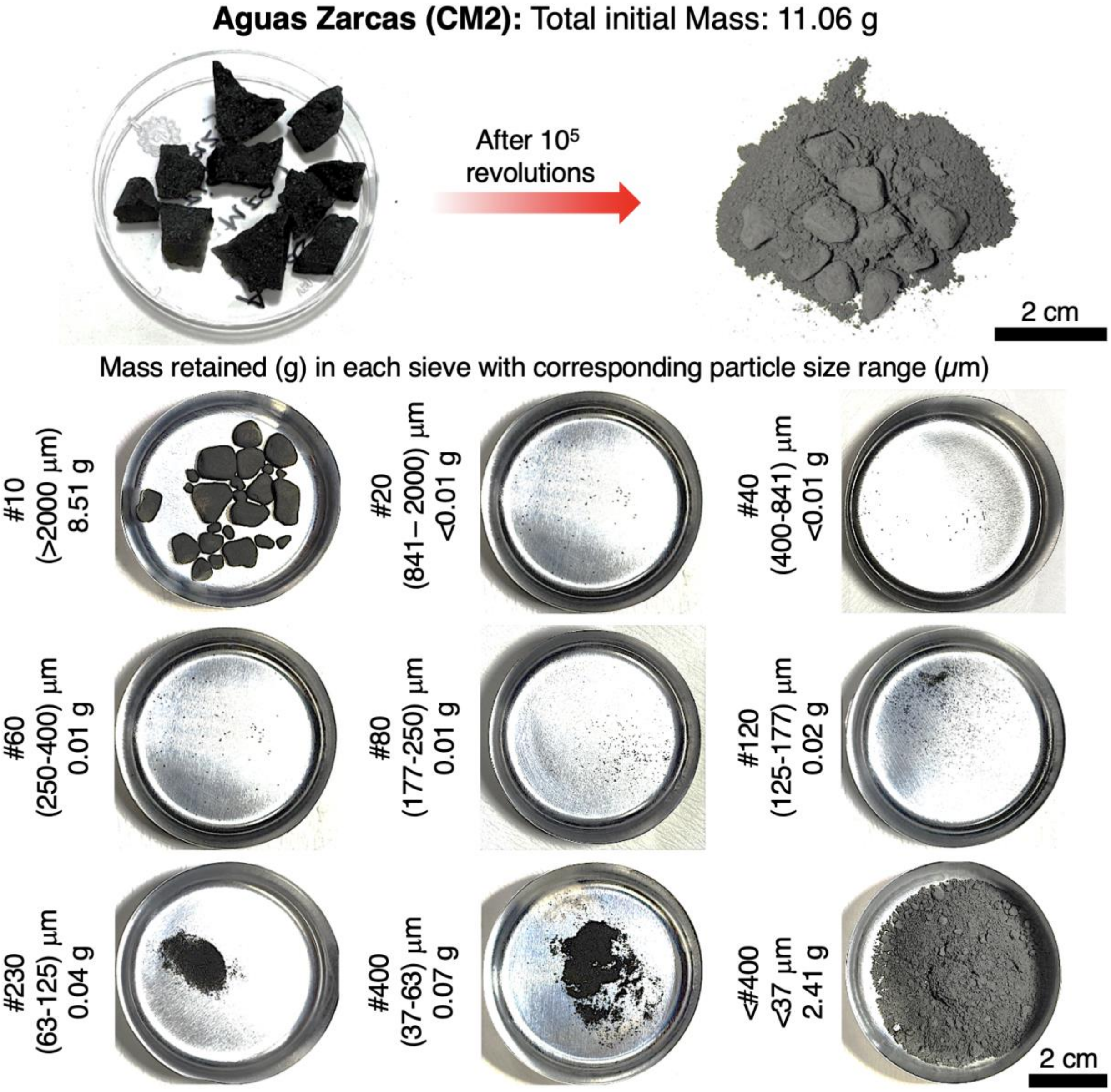

Supplementary Fig. 7: **Particle-size distribution of the Aguas Zarcas (CM2, low friability) meteorite after 10^5 revolutions.** An 11.06 g sample was subjected to mechanical tumbling and then analyzed by sieve separation. Most of the mass (~8.5 g) remains in the >2,000 µm bin, indicating high resistance to fragmentation. Only ~2.4 g was classified as <37 µm dust, with negligible mass in #20 - #120 sieve sizes.

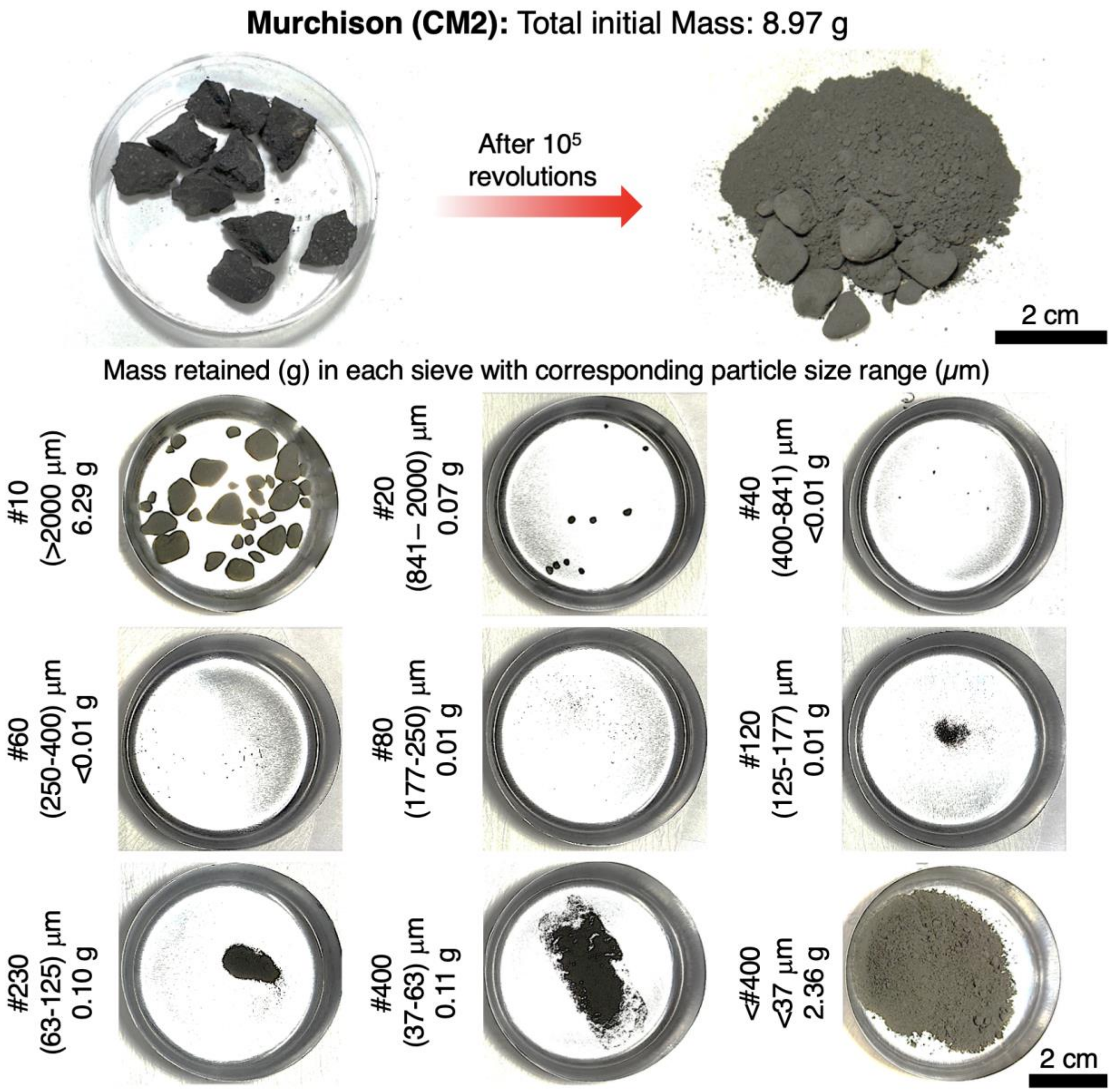

Supplementary Fig. 8: **Particle-size distribution of the Murchison (CM2, low friability) meteorite after 10^5 revolutions.** An 8.97 g sample was mechanically tumbled and analyzed using sieve separation. Most of the mass (~6.3 g) remains in the >2,000 μm bin, with ~2.4 g classified as <37 μm dust. #40 - #120 sieve bins retained minimal mass.

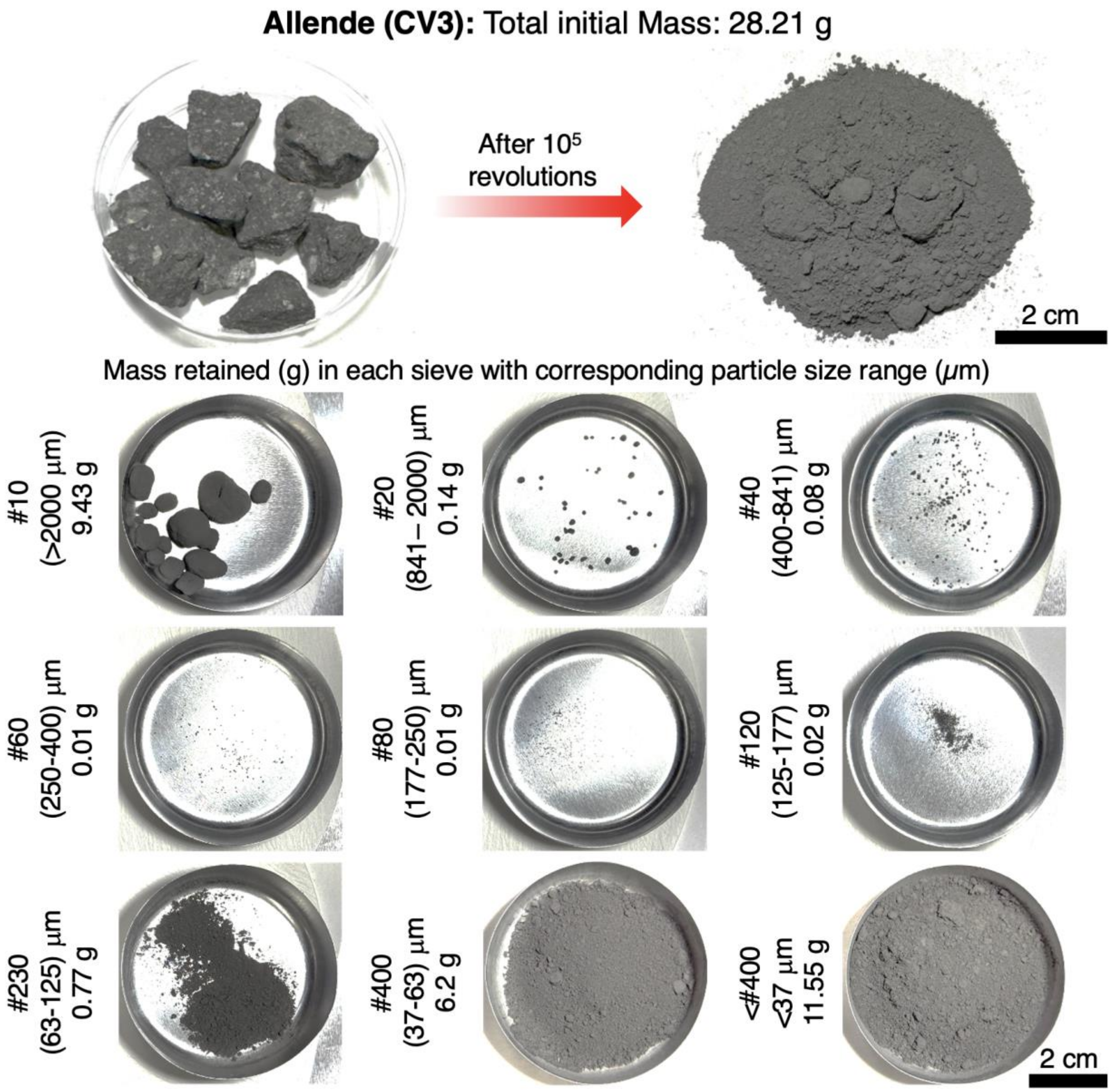

Supplementary Fig. 9: **Particle-size distribution of the Allende (CV3, medium friability) meteorite after 10^5 revolutions.** A 28.21 g sample was mechanically tumbled and subjected to a sieve analysis. While ~9.4 g remains in the >2,000 μm fraction, a substantial portion of the mass was redistributed into sand, including ~6.2 g in the 37–63 μm bin and ~11.6 g classified as <37 μm dust.

Supplementary Tables

Supplementary Table 1: Friability of meteorite samples across tumbling intervals. Cumulative mass fraction <2 mm for each meteorite sample after 10^1, 10^2, 10^3, 10^4, and 10^5 tumbler revolutions, expressed as the percentage of initial mass passing the 2 mm sieve. The data correspond to the curves in Fig. 2a.

Sample	Type	Initial Mass (g)	Friability (%) after				
			10^1 rev	10^2 rev	10^3 rev	10^4 rev	10^5 rev
Richardton	OC (H5)	13.20	8.00	28.13	59.08	84.03	96.68
Allende	CC(CV3)	28.21	0.22	1.79	9.61	31.20	66.56
Zhob	OC (H3-4)	13.40	0.72	1.99	8.33	26.54	65.39
New Concord	OC (L6)	12.37	0.29	1.44	6.05	20.68	63.33
Murchison	CC (CM2)	8.97	0.62	2.10	5.94	16.26	29.81
Aguas Zarcas	CC(CM2)	11.06	0.22	1.53	5.04	12.93	23.00
Tamdakht	OC (H5)	26.34	0.41	1.00	3.68	9.97	20.92

Supplementary Table 2: Sieve mass retention profiles of meteorite samples after progressive tumbling. Values represent the percent mass retained on each sieve size (µm) after 10^2, 10^3, 10^4, and 10^5 revolutions. Sieve bins are grouped into pebble (> 2,000 µm), sand (2,000–37 µm), and dust (< 37 µm). At 10^2 revolutions, most samples retain the greatest mass on the ~841 µm sieve, but with increasing revolutions, the dominant mass progressively shifts toward finer sizes, reflecting enhanced disaggregation. At 10^5 revolutions, the sand range converges toward chondrule-sized material, visualizing the mechanical pathway discussed in the Supplementary Discussion section.

# Revolutions	Fragment Size	#Sieve (µm)	Mass retained (%) for						
			Richardton	**Allende**	**Zhob**	**New Concord**	**Murchison**	**Aguas Zarcas**	**Tamdakht**
10^2	**Pebble**	**#10 (2000)**	**71.87**	**98.21**	**98.01**	**98.56**	**97.9**	**98.47**	**99**
	Sand	# 20 (841)	11.23	0.29	0.44	0.19	0.78	0.52	0.4
		#40 (400)	5.36	0.19	0.21	0.2	0.32	0.21	0.17
		#60 (250)	2.7	0.14	0.14	0.08	0.18	0.07	0.11
		#80 (177)	1.73	0.08	0.07	0.05	0.09	0.06	0.08
		#120 (125)	1.22	0.1	0.11	0.08	0.1	0.05	0.05
		# 230 (63)	1.44	0.17	0.18	0.15	0.11	0.05	0.05
		# 400 (37)	0.61	0.14	0.11	0	0.04	0	0.03
		Total Sand	**24.29**	**1.11**	**1.26**	**0.75**	**1.62**	**0.96**	**0.89**
	Dust	**<37**	**3.84**	**0.68**	**0.74**	**0.71**	**0.48**	**0.58**	**0.11**
10^3	**Pebble**	**#10 (2000)**	**40.92**	**90.39**	**91.67**	**93.95**	**94.06**	**94.96**	**96.32**
	Sand	# 20 (841)	18.63	0.94	1.1	0.58	0.97	1.04	0.9
		#40 (400)	11.97	0.47	0.96	0.27	0.38	0.23	0.45

		#60 (250)	6.23	0.38	0.55	0.09	0.28	0.12	0.19
		#80 (177)	4.57	0.28	0.33	0.05	0.23	0.09	0.12
		#120 (125)	2.93	0.38	0.33	0.06	0.37	0.11	0.17
		# 230 (63)	6.15	0.99	0.7	0.25	0.79	0.48	0.31
		# 400 (37)	0.05	1.09	0.91	0.62	0.57	0.41	0.24
		Total Sand	**50.53**	**4.53**	**4.88**	**1.92**	**3.59**	**2.48**	**2.38**
	Dust	**<37**	**8.53**	**5.08**	**3.45**	**4.13**	**2.34**	**2.56**	**1.32**
10^4	**Pebble**	**#10 (2000)**	**15.97**	**68.8**	**73.46**	**79.32**	**83.74**	**87.07**	**90.03**
	Sand	# 20 (841)	25.26	0.34	1.13	0.54	0.65	0.84	1.31
		#40 (400)	15.31	0.21	2.18	0.19	0.11	0.02	0.67
		#60 (250)	8.02	0.12	1.84	0.15	0.06	0.05	0.35
		#80 (177)	5.51	0.1	0.91	0.13	0.21	0.09	0.18
		#120 (125)	5.16	0.31	0.85	0.21	0.24	0.16	0.26
		# 230 (63)	4.76	2.23	1.69	0.54	1.15	1.29	0.29
		# 400 (37)	4.33	9.55	3.05	1.61	3.77	2.73	0.42
		Total Sand	**68.35**	**12.86**	**11.65**	**3.37**	**6.19**	**5.18**	**3.48**
	Dust	**<37**	**15.68**	**18.34**	**14.89**	**17.32**	**10.08**	**7.76**	**6.49**
10^5	**Pebble**	**#10 (2000)**	**3.32**	**33.44**	**34.61**	**36.67**	**70.19**	**77**	**79.08**
	Sand	# 20 (841)	17.59	0.49	0.84	1.93	0.74	0	1.03

		#40 (400)	23.61	0.27	3.75	0.81	0.01	0	1.01
		#60 (250)	10.08	0.04	4.7	0.57	0.03	0.03	1.06
		#80 (177)	4.72	0.03	1.89	0.43	0.09	0.06	0.32
		#120 (125)	5.03	0.08	1.69	0.49	0.22	0.15	0.36
		# 230 (63)	7.12	2.73	3.04	0.72	1.17	0.37	0.3
		# 400 (37)	5.26	21.96	9.59	1.16	1.2	0.59	0.22
		Total Sand	**73.41**	**25.6**	**25.5**	**6.11**	**3.46**	**1.2**	**4.3**
	Dust	**<37**	**23.28**	**40.95**	**39.9**	**57.22**	**26.35**	**21.81**	**16.61**

Supplementary Reference:

1. Cotto-Figueroa, D. *et al.* Scale-dependent measurements of meteorite strength: Implications for asteroid fragmentation. *Icarus* **277**, 73–77 (2016).
2. Mason, B. H. & Wiik, H. B. (Hugo B. The composition of the Richardton, Estacado, and Knyahinya meteorites. American Museum novitates ; no. 2154. http://hdl.handle.net/2246/3333 (1963).
3. Quirke, T. T. The Richardton Meteorite. *J. Geol.* **27**, 431–448 (1919).
4. Meteoritical Bulletin: Entry for Tamdakht. https://www.lpi.usra.edu/meteor/metbull.php?code=48691 (2009).
5. Meteoritical Bulletin: Entry for Zhob. https://www.lpi.usra.edu/meteor/metbull.php?code=71596 (2021).
6. Mason, B. & Wiik, H. B. (Hugo B. The composition of the Ottawa, Chateau-Renard, Mocs, and New Concord Meteorites. in (American museum of natural history, New York, NY, 1961).
7. mindat.org. New Concord meteorite. https://www.mindat.org/loc-269392.html.
8. Fendrich, K. V. & Ebel, D. S. Comparison of the Murchison CM2 and Allende CV3 chondrites. *Meteorit. Planet. Sci.* **56**, 77–95 (2021).
9. Scott, E., Keil, K. & Stöffler, D. Shock metamorphism of carbonaceous chondrites. *Geochim. Cosmochim. Acta* **56**, 4281–4293 (1992).
10. Lee, S., Keller L. P., Morris, R. V., Han, J. & Rahman, Z. Thermal decomposition of the murchison CM2 carbonaceous chondrite: Implications of space weathering processes for sample return missions. (2020).
11. Floyd, C. J. *et al.* Chondrule sizes within the CM carbonaceous chondrites and measurement methodologies. *Meteorit. Planet. Sci.* **59**, 2769–2788 (2024).

12. Garvie, L. A. J. Mineralogy of the 2019 Aguas Zarcas (CM2) carbonaceous chondrite meteorite fall. *Am. Mineral.* **106**, 1900–1916 (2021).

13. Russell, S. S. & Howard, L. The texture of a fine-grained calcium-aluminium-rich inclusion (CAI) in three dimensions and implications for early solar system condensation. *Geochim. Cosmochim. Acta* https://www.researchgate.net/publication/258646152_The_texture_of_a_fine-grained_calcium-aluminium-rich_inclusion_CAI_in_three_dimensions_and_implications_for_early_solar_system_condensation (2012).

14. Keller, L. P. & Buseck, P. R. Twinning in meteoritic and synthetic perovskite. *Am. Mineral.* **79**, 73–79 (1994).

15. Krot, A. N., Scott, E. R. D. & Zolensky, M. E. Mineralogical and chemical modification of components in CV3 chondrites: Nebular or asteroidal processing? *Meteoritics* **30**, 748–775 (1995).

16. Scott, E. R. D., Barber, D. J., Alexander, C. M., Hutchinson, R. & Peck, J. A. *Primitive Material Surviving in Chondrites: Matrix. Meteorites and the Early Solar System* 718–745 (1988).

17. Toriumi, M. Grain size distribution of the matrix in the Allende chondrite. *Earth Planet. Sci. Lett.* **92**, 265–273 (1989).